ARTICLE

Vibrational Mode Selectivity in Dissociative Ionization of 2-Ethoxyethanol: An IR-VUV NRIFD-IR Spectroscopic Study

Licheng Zhong[a,b], Ende Huang[b,c], Guosheng Wang[a*], Jingning Xue[b,d], Wenrui Dong[b,e*], Xueming Yang[b,f]

a. College of Chemical Engineering, Shenyang University of Chemical Technology, Shenyang 110142, China
b. State Key Laboratory of Molecular Reaction Dynamics, Dalian Institute of Chemical Physics, Chinese Academy of Sciences, Dalian 116023, China
c. University of Chinese Academy of Sciences, Beijing 100049, China
d. Department of Physics, School of Science, Dalian Maritime University, Dalian 116026, China
e. Hefei National Laboratory, Hefei 230088, China
f. Department of Chemistry, Southern University of Science and Technology, Shenzhen 518055, China

(Dated: Received on April 2, 2024; Accepted on May 19, 2024)

In the current work, we studied the infrared spectroscopy of neutral and cationic 2-ethoxyethanol (CH_3CH_2O CH_2CH_2OH, 2-EE) using the infrared (IR)–vacuum-ultraviolet (VUV) nonresonant ionization and fragmentation detected IR spectroscopy (NRIFD-IR) technique. The spectral range was from 2700 cm^{-1} to 7250 cm^{-1}. Upon radiation with a 118 nm laser, signals corresponding to the cationic 2-EE (m/z=90) and dissociative ionization products (m/z=72, 59, 46, and 45) were detected. The action IR spectra, derived from the signal variations of 2-EE and its fragments upon IR radiation, display differences, suggesting vibrational mode selectivity in the dissociative ionization process. To complement the experimental findings, we performed density functional theory calculations at the B3LYP-D3(BJ)/def2-TZVPP level to determine the structures and anharmonic IR spectra of neutral and cationic 2-EE. The computed spectra showed good agreement with the experimental results.

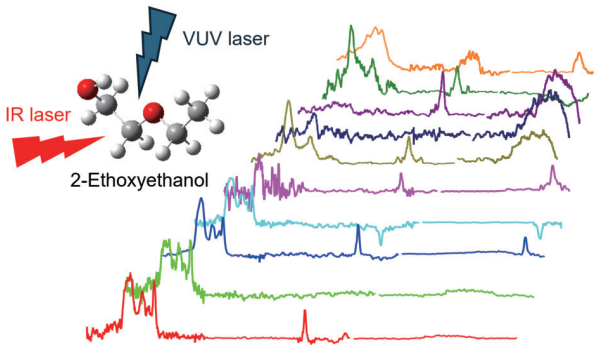

Key words: Gas phase infrared spectroscopy, Neutral and cationic molecular structure, Vibrational mode selectivity

I. INTRODUCTION

2-Ethoxyethanol (2-EE), also known as ethylene glycol ethyl ether, is a versatile chemical compound with a wide range of applications, including its use as a solvent, cleaning agent, chemical intermediate, and in various industries such as ink, textile, and pharmaceuticals [1]. 2-EE has been reported as one of the major volatile organic compounds (VOCs) emitted from vehicles using diesel/biodiesel blends as fuel [2]. Due to its presence in the atmosphere, the reactivities of 2-EE with atmospheric oxidants, such as OH, NO_3, and Cl, have been investigated to understand its atmospheric implications [3–5].

Experimental data on the IR spectrum of 2-EE in the gas phase are scarce, notwithstanding the significance of this compound. Moreover, few theoretical studies have been conducted to investigate the dissociation path-

* Authors to whom correspondence should be addressed. E-mail: wangguosheng@syuct.edu.cn, wrdong@dicp.ac.cn

ways and resulting ionic fragments following the ionization of 2-EE molecules. However, the IR spectrum of a similar molecule, 2-methoxyethanol (2-ME), has been extensively studied in liquid [6–9], Ar matrix isolation [10], and gas phase conditions [11]. These studies have utilized the IR spectrum to identify the conformations of 2-ME in different conditions. For example, in the liquid state, 2-ME exists in both *gauche*-(anti-*gauche*)-*trans* and minor *trans-trans-trans* conformations [6–9]. However, under the gas phase and Ar matrix isolation conditions (11–44 K), only the most stable *gauche*-(anti-*gauche*)-*trans* conformation is present [10, 11]. Interestingly, the IR spectrum of the 2-ME cation is dominated by the second stable conformer, which is attributed to the redistribution of surplus energy (approximately 0.37 eV) from the photoionization process to the internal energy of the cationic form of 2-ME [11]. Furthermore, the C–H stretch fundamental band of the 2-ME cation is blue shifted by around 100 cm^{-1} in comparison with its neutral counterpart. This shift is attributed to the interaction of $n(O)\rightarrow\sigma^*(C_\alpha H)$ weakening the C_α–H bond of the neutral form, as indicated by the natural bond orbital (NBO) analysis [11].

Under ionization conditions close to the threshold, the VUV laser could detect the gas phase species with high efficiency, minimizing complications caused by fragmentation. Therefore, the combination of VUV laser, supersonic beam, and mass spectrometry (MS) with IR laser has proven to be a powerful approach to investigating the structures of gas phase species [12, 13], analyzing specific sizes and conformations, such as those of water [14, 15], alcohols [16, 17], ammonia [18, 19], acetone [20, 21], and pyridine [22].

In the present research, the infrared (IR)-vacuum-ultraviolet (VUV) non-resonant ionization and fragmentation detected IR (NRIFD-IR) spectroscopy was utilized to determine the IR spectra of both neutral and positively charged 2-EE. In the NRIFD-IR technique, a VUV laser was utilized for single-photon ionization or dissociative ionization of neutral species. For the IR spectra of neutral species, the IR laser pulse preceded the VUV laser pulse, while for the IR spectra of positively charged species, the IR laser pulse followed the VUV laser pulse. The IR spectra were derived from the difference between the signals of the target species, or its fragments, with and without IR radiation. By monitoring the fluctuations in the signal intensities of neutral 2-EE (m/z=90) and its dissociative ionization products (m/z=72, 59, 46, and 45) upon exposure to 118 nm radiation, with and without the absorption of IR radiation, we acquired the IR spectra of neutral and cationic forms of 2-EE. The experimentally observed IR spectra were compared with the computed spectra employing density functional theory (DFT) calculations to propose the major spectral contributors for the neutral and positively charged 2-EE.

II. EXPERIMENTAL AND THEORETICAL METHODS

A. Experimental methods

The IR absorption spectra of neutral and positively charged 2-EE were acquired by observing the variations in the signal intensities of 2-EE (m/z=90) and its dissociative ionization fragments m/z=72, 59, 46, and 45. This was achieved by scanning the IR radiation frequency, which was timed to arrive either preceding (for neutral 2-EE) or succeeding (for positively charged 2-EE) the 118 nm laser pulse. The 118 nm laser was obtained through frequency tripling of a 355 nm laser (approximately 40 mJ/pulse), resulting from the third-harmonic generation of a Nd:YAG laser operating at 20 Hz (Beamtech, SGR-20). Xenon and argon, with a ratio of 1:10, were contained within a pressurized cell at approximately 300 Torr. This gaseous mixture facilitated the generation of a 118 nm laser. A magnesium fluoride (MgF_2) plano-convex lens was installed at the end of the gas cell to focus the 118 nm laser beam into the detection area.

An optical parametric oscillator/amplifier (OPO/OPA) system from Laser Vision was employed to generate tunable IR radiation with a linewidth of 0.9 cm^{-1}. A Nd:YAG laser (Continuum, Surelite EX, unseeded, 10 Hz, 630 mJ/pulse) was employed to pump the OPO/OPA system. The typical energy of the IR laser at the calcium fluoride (CaF_2) window, located at the entrance of the vacuum chamber, was 10 mJ per pulse with a pulse duration of 6 ns. A CaF_2 lens with a focal length of 500 mm was employed to focus the beam into the detection area, where ionization occurs.

2-EE (99%, Sigma-Aldrich) was soaked in glass fiber filter paper, which was put in a sample cartridge inside the Even Lavie valve, operating at a repetition rate of 20 Hz. The molecular beam consisted of approximately 0.03% 2-EE in argon, with the Ar back pressure of 250 psi and vapor pressure of about 0.073 psi at room temperature. The molecular beam, after being collimat-

DOI: 10.1063/1674-0068/cjcp2403045

ed by a skimmer with a diameter of 1.5 mm positioned approximately 2 cm downstream from the nozzle, intersected perpendicularly with the 118 nm VUV laser within the ionization zone.

The IR and VUV laser beams propagated in a counter direction and overlapped in the detection area. The IR laser was timed to proceed (50 ns) or follow (70 ns) the VUV laser to obtain the IR spectrum of neutral or cationic 2-EE. The analog-to-digital converter (ADC) card (Acqiris, 2 GS/s) received the ion signal after it was amplified by a Stanford Research Systems SR445A amplifier. The digitized signal was then recorded and stored on a computer for further analysis. The IR spectrum was obtained through the subtraction of the signal generated by VUV single-photon ionization (IR off) from the signal generated by the combination of the IR and VUV laser (IR on).

B. Theoretical methods

To ascertain the minimum energy conformation of the 2-EE molecule, a multi-step approach was employed, combining various computed methods and levels of theory. First, the Molclus software [23] was employed to perform systematic conformational analyses to determine potential conformers. This process yielded 32 candidate structures, which were then subjected to preliminary geometry optimizations using density functional theory (DFT) with Grimme's dispersion correction, Becke-Johnson damping, and three-body terms D3(BJ) [24–26] at the B3LYP/def2-TZVPP level, using the Gaussian 16 program suite [27]. The inclusion of dispersion corrections is crucial for accurately describing non-covalent interactions, including hydrogen bridging and van der Waals forces, which exert a profound influence on determining the conformational preferences of molecules like 2-EE.

The preliminary optimization process resulted in the identification of 11 stable conformers of neutral 2-EE. To ensure the reliability of the obtained structures, these conformers were further reoptimized at the same level of theory, B3LYP-D3(BJ)/def2-TZVPP. This two-step optimization approach helps to refine the geometries and energies of the conformers. The conformational search and optimization procedures were carried out for the cationic species, leading to the identification of 11 distinct cationic 2-EE structures.

Vibrational analysis offers a potent means of characterizing the structural and spectroscopic properties of molecules. Vibrational analysis was performed on the neutral and positively charged 2-EE structures at the B3LYP-D3(BJ)/def2-TZVPP level to acquire the zero-point energies (ZPE). To further refine the energies of the optimized structures, single-point energy computations were performed utilizing a higher level of theory, employing the RIJK-CCSD(F12*)(T*)/cc-pVTZ-F12 method in conjunction with the ORCA program [28]. The single-point energies were corrected with the previously obtained ZPE values to yield the final ZPE-corrected energies for both the neutral and cationic 2-EE conformers.

Finally, to simulate the anharmonic IR absorption spectra of the neutral and positively charged 2-EE, the vibrational second-order perturbation theory (VPT2) methodology was employed, as incorporated within the Gaussian 16 software package, at the B3LYP-D3(BJ)/def2-TZVPP level of theory. The VPT2 method accounts for anharmonic effects in the vibrational motion of the molecule, providing a more realistic representation of the IR spectra compared to the harmonic approximation. By simulating the IR spectra, one can gain insights into the vibrational modes and spectroscopic signatures of the 2-EE molecule in both its neutral and cationic forms, which can be valuable for experimental characterization and comparison.

III. RESULTS AND DISCUSSION

A. 118 nm photoionization and dissociative ionization products of 2-EE

FIG. 1 presents the 118 nm photoionization and dissociative ionization products of 2-EE, in the presence of (red) and absence of (black) the IR radiation at 2880 cm^{-1}. The vertical ionization energy (VIE) of 2-EE is reported to be 9.97 eV [29], and among the dissociative ionization products, only the appearance energy (AE) of the $C_3H_7O^+$ (m/z=59) is known, which is 10.26 eV [30].

The mass spectrum generated through the application of an IR laser at a frequency of 2880 cm^{-1}, 50 ns before the 118 nm laser, shows changes in the signal of fragments with mass-to-charge ratios m/z=89, 72, 59, 46, and 45 compared to the mass spectrum from VUV ionization alone. The elimination of a water molecule from the cationic 2-EE is a plausible pathway for the generation of the dominant fragment, m/z=72. It can proceed through two distinct pathways. The first path-

DOI: 10.1063/1674-0068/cjcp2403045

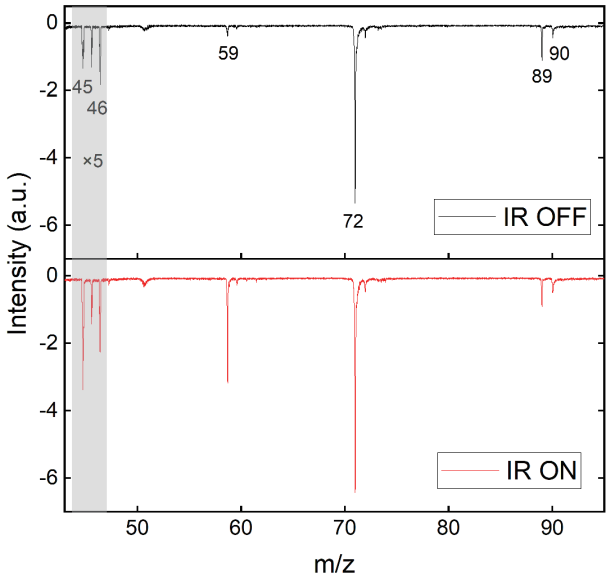

FIG. 1 Mass spectra of 2-EE, along with its dissociative ionization products, observed with the 118 nm laser. The spectra were taken with the absence or presence of an IR laser (2880 cm^{-1}).

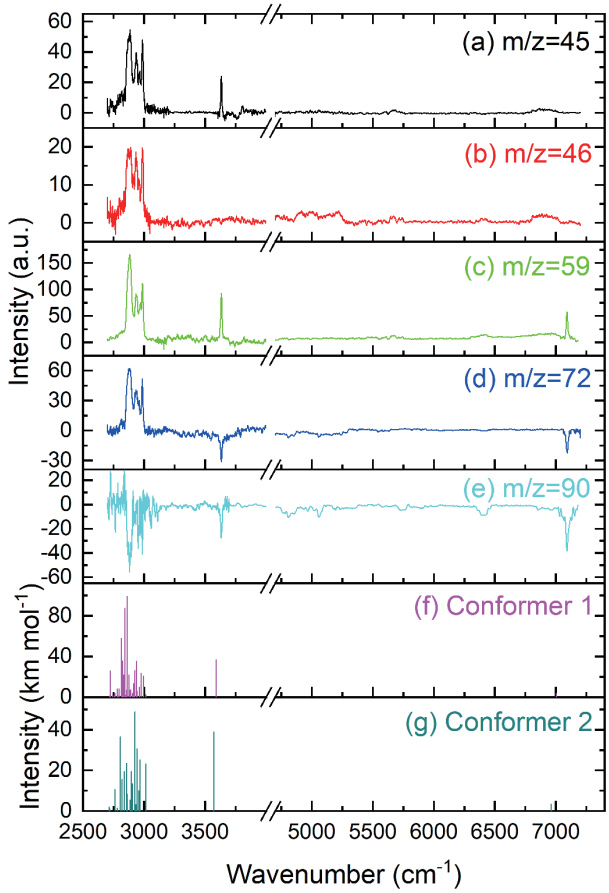

FIG. 2 The NRIFD-IR vibrational spectra of neutral 2-EE within the wavenumber range of 2700−7200 cm^{-1}, along with the calculated IR spectra of the two most stable conformers.

way involves the removal of water from the carbon atom neighboring the etheric oxygen of 2-EE, resulting in the formation of $[CH_2{=}CHOCH_2CH_3]^+$. Alternatively, the second pathway entails the migration of a hydrogen atom from the methyl group to the terminal hydroxyl group (OH) preceding the scission of the carbon-oxygen (C−O) covalent bond, forming the tetrahydrofuran cation. These two pathways are analogous to the water elimination process of 2-methoxyethanol [31, 32].

The fragment m/z=89 is attributed to the parent cation losing a hydrogen atom. The fragment m/z=59 ($[CH_3CH_2OCH_2]^+$) is formed by the loss of a hydroxymethyl group (CH_2OH) from the parent ion. An estimation based on the potential energy diagram [33], suggests that the AE of this channel is approximately 10.64 eV, which is consistent with the current observation, considering the uncertainty in the calculation.

The fragment m/z=46 could be formed through two possible pathways: transfer of either the hydroxyl hydrogen or the hydroxymethyl hydrogen to the oxygen atom within the ether linkage, subsequently leading to the scission of the C−O bond between the ethoxy and ethanol moieties, forming the $[CH_3CH_2OH]^+$.

Lastly, the formation of the fragment with m/z=45 can be ascribed to two possible mechanisms. The first pathway involves the scission of the C−O bond connecting the ethoxy group and the ethanol moiety, generating an ethoxy cation with the formula $[CH_3CH_2O]^+$. Subsequently, this cation undergoes a rearrangement process known as a 1,2-hydrogen shift, leading to the formation of a more stable isomeric species, $[CH_3CHOH]^+$. The second pathway involves the loss of a methylene hydrogen, followed by the migration of the hydrogen atom from CH_2OH to the oxygen atom in the ether bond, and the subsequent scission of the C–O covalent bond, yielding the $[CH_3CHOH]^+$.

B. IR spectra of neutral 2-EE

The NRIFD-IR vibrational spectra of neutral 2-EE within the wavenumber range of 2700−7200 cm^{-1}, along with the calculated IR spectra, are depicted in FIG. 2. The IR enhancement spectra, acquired from observing fragments m/z=45, 46, and 59 are shown in FIG. 2(a−c), while the IR dip spectrum detected by the parent cation m/z=90 is illustrated in FIG. 2(e). The spectrum in FIG. 2(d), obtained by detecting the m/z=72 fragment, exhibits enhancement in the IR

DOI: 10.1063/1674-0068/cjcp2403045

TABLE I The anharmonic vibrational wavenumbers of the most stable conformer of 2-EE were computed using the B3LYP-D3(BJ)/def2-TZVPP method. Note that only absorption peaks between 2850 and 7150 cm^{-1} with absorption intensities surpassing 6 km/mol are shown. All absorption peaks with absorption intensities exceeding 1 km/mol can be found in Table S1 of Supplementary materials.

Vibrational mode	Experimental frequency/cm^{-1}	Calculation	
		Anharmonic frequency/cm^{-1}	Mode description
ν_4	2880	2876(116.10)	OCC asym CH str.
$\nu_{11}+\nu_{10}$		2900(25.19)	COC sym CO str., CC str.
ν_3		2914(20.47)	CH_3 sym CH str.
$2\nu_{10}$		2920(11.38)	CC str.
$\nu_{11}+\nu_9$		2922(6.52)	COC sym CO str., CH rocking
$\nu_{10}+\nu_{13}$	2937	2935(15.02)	CC str., COC sym CO str.
$\nu_{13}+\nu_9$		2960(7.42)	COC sym CO str., CH rocking
$2\nu_9$		2971(7.02)	CH rocking
ν_2	2989	2977(26.57)	CH_3 asym CH str.
ν_1	3634	3652(29.17)	OH str.
$2\nu_1$	7092	7130(6.89)	OH str.

range of 2845−3010 cm^{-1} and reduction at IR absorption higher than 3600 cm^{-1}. The simulated infrared vibrational frequencies, incorporating anharmonic corrections, at the B3LYP-D3(BJ)/def2-TZVPP level of theory for the two most energetically favored conformational isomers of 2-EE are depicted in FIG. 2(f, g). It is noteworthy that all the experimental spectra in FIG. 2 were acquired with the IR laser introduced to the ionization area 50 ns preceding the 118 nm laser, thus representing the IR absorption of neutral 2-EE.

In the region of 2750−3050 cm^{-1}, all the experimental spectra exhibited three prominent vibrational bands with their maxima situated at 2880, 2937, and 2989 cm^{-1} (FIG. 2(a−e)). The absorption at 2880 cm^{-1} is primarily attributed to the OCC antisymmetric CH stretch transition, with possible contributions from transitions calculated to be located in the range of 2847−2899 cm^{-1}, as presented in Table I. According to the calculation, several relatively strong absorptions are present in the vicinity of the peak at 2937 cm^{-1}, with one or more potentially contributing to the observed absorption. The calculated combination mode of the C−C stretch and the C−O−C symmetric C−O stretch (2935 cm^{-1}) is the closest to the observed peak. The absorption band observed at 2989 cm^{-1} is the narrowest among the three peaks and is mainly attributed to the methyl antisymmetric CH stretch transition, considering the calculated peak intensity and position.

The peak at 3634 cm^{-1} corresponds to the OH stretch transition, which was calculated to be at 3652 cm^{-1}. All experimental spectra show this peak, except for the spectrum from observing the fragment m/z=46, as shown in FIG. 2(b). This could be due to the incompleteness of the intramolecular vibrational redistribution (IVR), thus exhibiting vibrational mode selectivity in the dissociative ionization of neutral 2-EE upon IR excitation and VUV ionization. In section III.A, we have proposed two possible pathways to generate the m/z=46 fragment. The pathway that involves the transfer of the hydroxyl hydrogen to the oxygen atom in the ether bond prior to the cleavage of the C−O bond will be facilitated by the OH stretch excitation, thus increasing the intensity of the m/z=46 fragment. The absence of the peak at 3634 cm^{-1} in FIG. 2(b) suggests that the dissociative ionization of 2-EE to the m/z=46 fragment occurs via the transfer of the hydroxymethyl hydrogen to the oxygen atom in the ether bond, subsequent to the scission of the C−O bond between the ethoxy and ethanol moieties. In this case, the energy of the excited OH stretch mode may not be sufficiently redistributed, and thus does not contribute to the dissociative ionization.

The observed vibrational mode selectivity provides insights into the dissociative ionization mechanisms and the specific bond cleavage processes involved in the fragmentation process of 2-EE. It suggests that the selective excitation of different vibrational modes can promote or inhibit certain fragmentation pathways, depending on the vibrational modes excited and the subsequent energy redistribution. A detailed understand-

DOI: 10.1063/1674-0068/cjcp2403045

ing of the potential energy surfaces and the coupling between different vibrational modes is crucial for accurately predicting and interpreting the fragmentation patterns observed in the NRIFD-IR experiments.

In FIG. 2(d), the signal intensity of the fragment with m/z=72 decreases upon the absorption of 3634 cm^{-1} IR radiation by neutral 2-EE prior to ionization by VUV laser, in contrast to the behavior exhibited in the region of 2750−3050 cm^{-1}. This suggests that with the additional energy provided by 3634 cm^{-1} IR photons, the 2-EE cation, ionized by 118 nm radiation, favors the formation of other fragments over the m/z=72 fragment. A similar trend is observed when neutral 2-EE absorbs IR radiation of 7092 cm^{-1}.

The IR spectra of the m/z=72 and 59 fragments, as well as that of the parent cation, show a peak at 7092 cm^{-1}, which is attributed to the overtone transition of the OH stretching mode. However, this peak is not observed in the spectra of the m/z=46 and m/z=45 fragments. The absence of the peak in the m/z=46 fragment can be explained by the same reason as the absence of the peak at the fundamental OH stretch transition (3634 cm^{-1}). On the other hand, the lack of a peak in the m/z=45 fragment can potentially be ascribed to the energy-dependent behavior of this channel. As the overall energy of the system increases (in this case, the increase in the energy of the IR photon), the formation of the m/z=45 fragment becomes less favored. Coincidentally, at the 7092 cm^{-1} IR excitation, the signal intensity of the m/z=45 fragment remains unchanged regardless of the presence or absence of the IR photon. This behavior is in contrast to the signal intensity of the m/z=72 channel, which shows enhancement at lower IR photon energies but reduction at the IR photon energy of 7092 cm^{-1}.

The computed IR spectrum of the two most stable 2-EE conformers is shown in FIG. 2 (f) and (g). The IR spectrum of the lowest-energy conformer displayed superior congruence with the experimental observation across the entire spectra region (2700−7200 cm^{-1}), in terms of both peak position and intensity. It is reasonable, considering that the spectra carrier is dominated by the most stable conformer. In the supersonic molecular beam, the 2-EE molecules undergo severe collisions, which should provide sufficient cooling for the molecules to distribute into the lowest-energy conformer. The structures of the two lowest-energy neutral 2-EE conformers are shown in FIG. S1 in SM. The energy difference between those two conformers is calculated to be 1.88 kcal/mol.

C. IR spectra of cationic 2-EE and its fragments

In the measurement of IR spectra for neutral 2-EE, the IR laser pulse preceded the VUV laser pulse by 50 ns, arriving at the ionization region earlier. Consequently, all the peaks in the IR spectra, whether by detecting 2-EE or its fragments, represent the IR absorption of neutral 2-EE. In contrast, during the measurement of the cationic 2-EE spectrum, the IR pulse was delayed by 70 ns relative to the VUV radiation. As a result of the 118 nm VUV radiation, both the 2-EE cation and its cationic fragments are present when the IR laser arrives. Therefore, the IR laser can dissociate not only the 2-EE cation but also the cationic fragments.

The variation in signal intensity of a specific cationic fragment upon IR radiation can thus originate from the IR dissociation of the 2-EE cation, the cationic fragments with larger m/z than the detected cationic fragment, and the cationic fragment itself. This fact complicates the observed IR spectra, making it more challenging to attribute the IR absorption to specific species.

The NRIFD-IR vibrational spectra of the positively charged 2-EE, spanning the frequency range from 2700 cm^{-1} to 7050 cm^{-1}, were acquired and compared with the computed results (FIG. 3). In the 2700−3200 cm^{-1} region, the IR spectrum of cationic 2-EE (FIG. 3(e)) features a broad peak with a tail extending beyond 2700 cm^{-1}. Three weakly resolved peaks at 2909, 2948, and 2995 cm^{-1} are observed, which are in proximity (within 10 cm^{-1}) to the calculated wavenumbers of the methyl symmetric CH stretching mode, HOCC symmetric CH stretching mode, and methyl antisymmetric CH stretching mode, respectively (Table II). The low wavenumber tail of the peak can be attributed to several transitions, primarily combination modes (Table S2 in SM), with moderate absorption intensities in the 2750−2900 cm^{-1} range.

The peaks centered at 3574 and 6938 cm^{-1} are assigned to the fundamental and overtone transitions of the OH stretching mode. The calculated IR spectra of the two lowest-energy conformational isomers of the positively charged 2-EE show minimal differences. However, the calculated fundamental and overtone OH stretch transitions of the lowest-energy conformational isomer display a closer correlation with the observed peak center positions. It is important to note that the

DOI: 10.1063/1674-0068/cjcp2403045

TABLE II The anharmonic vibrational wavenumbers of the most stable conformer of cationic 2-EE were calculated using the B3LYP-D3(BJ)/def2-TZVPP method. Note that only absorption peaks between 2900 and 7000 cm^{-1} with intensities stronger than 1 km/mol are shown. All absorption peaks with intensities greater than 0.5 km/mol can be found in Table S2 of SM.

Vibrational mode	Experimental frequency/cm^{-1}	Calculation	
		Anharmonic frequency/cm^{-1}	Mode description
ν_5		2916(2.55)	HOCC sym CH str.
ν_4	2909	2919(7.21)	CH_3 sym CH str.
ν_6	2948	2959(2.82)	HOCC sym CH str.
ν_3	2995	2998(4.16)	CH_3 asym CH str.
ν_1	3574	3552(261)	OH str.
$2\nu_1$	6938	6935(10.75)	OH str.

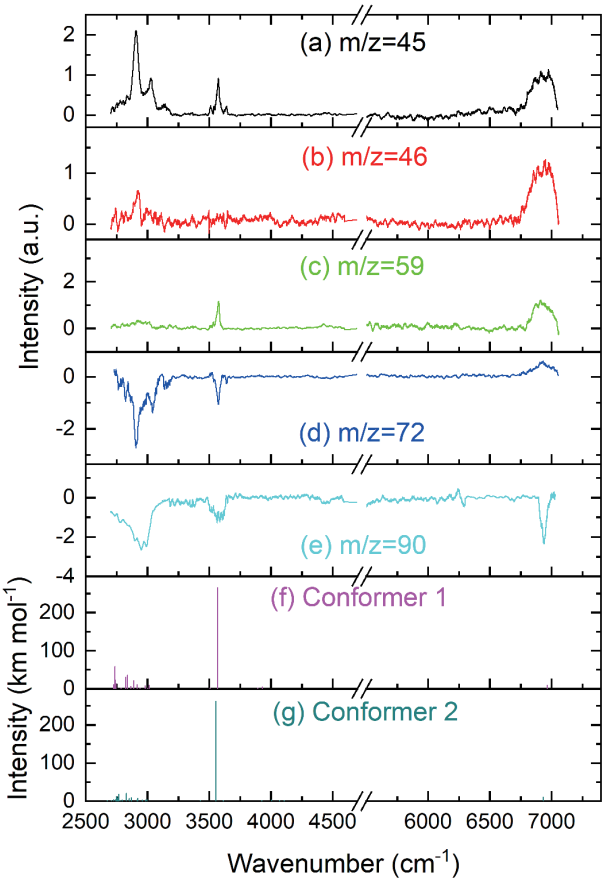

FIG. 3 The NRIFD-IR vibrational spectra of cationic 2-EE and its fragments in the range of 2700−7050 cm^{-1}, along with the calculated IR spectra of the two most stable conformers.

two conformers have an energy difference of 0.63 kcal/mol, and considering the excess energy of approximately 12 kcal/mol in the cationic 2-EE after ionization by the 118 nm laser (the vertical ionization energy of 2-EE is reported to be 9.97 eV [29]), it is highly likely that both conformers contribute to the observed IR spectra.

FIG. 3(a−e) show obvious peaks centered at 6938 cm^{-1}, which corresponds to the overtone of the OH stretch transition. Both FIG. 3 (a) and (c) exhibit two peaks at 2909 and 3035 cm^{-1}, with matching relative intensities, suggesting that the majority of the cationic fragment of m/z=45 in the region of 2800−3200 cm^{-1} originates from the IR dissociation of the cationic fragment of m/z=72. FIG. 3(c) illustrates that the signal intensity of the cationic fragment of m/z=72 decreases upon IR radiation, indicating that the dissociation of this fragment by IR radiation cannot be compensated by the IR dissociation of the cationic 2-EE.

The IR spectrum of the m/z=46 fragment channel does not show a peak at the position corresponding to the OH stretch transition and exhibits weak peaks in the region of 2700−3200 cm^{-1}. In contrast, the IR spectrum of the m/z=59 fragment channel shows a broad peak between 2700 and 3200 cm^{-1}, similar to the profile in FIG. 3(e), indicating that the cationic fragment of m/z=59 in this region might originate from the IR dissociation of the cationic 2-EE.

IV. CONCLUSION

In summary, we employed the NRIFD-IR technique to explore the vibrational spectra of neutral and cationic 2-EE in the 2700−7250 cm^{-1} range. The IR spectra of neutral 2-EE exhibited distinct peaks corresponding to various vibrational modes. The observed differences in the IR spectra of the dissociative ionization products highlighted the vibrational mode selectivity in the dissociative ionization process. Additionally, we investigated the IR spectra of cationic 2-EE and its fragments, revealing broad peaks and distinct transitions associated with various vibrational modes, demonstrating the intricate nature of the observed IR spectra, particularly in the context of the dissociation of cationic fragments

DOI: 10.1063/1674-0068/cjcp2403045

by IR radiation. The experimental results were supported by density functional theory calculations at the B3LYP-D3(BJ)/def2-TZVPP level, which provided consistent theoretical spectra.

Supplementary materials: Optimized stable structures of neutral and cationic 2-ME, predicted IR transitions of the most stable conformer of neutral and cationic 2-ME are shown.

V. ACKNOWLEDGMENTS

The authors gratefully acknowledge the Dalian Coherent Light Source (DCLS) for support and assistance. This work was funded by the National Natural Science Foundation of China (No.22288201), the Chinese Academy of Sciences (GJJSTD20220001), and the Innovation Program for Quantum Science and Technology (No.2021ZD0303305).

[1] K. Stemmler, W. Mengon, and J. A. Ker, Environ. Sci. Technol. **30**, 3385 (1996).
[2] M. J. O'Neil, *The Merck Index: An Encyclopedia of Chemicals, Drugs, and Biologicals* (15th Edn.), Cambridge: Royal Society of Chemistry, (2013).
[3] I. Colmenar, S. Salgado, P. Martín, I. Aranda, A. Tapia, and B. Cabañas, Atmos. Environ. **224**, 117367 (2020).
[4] H. M. Yu, K. H. Møller, R. S. Buenconsejo, J. D. Crounse, H. G. Kjaergaard, and P. O. Wennberg, J. Phys. Chem. A **127**, 9564 (2023).
[5] K. Stemmler, W. Mengon, and J. A. Kerr, Environ. Sci. Technol. **30**, 3385 (1996).
[6] F. A. J. Singelenberg, J. H. Van Der Maas, and L. M. J. Kroon-Batenburg, J. Mol. Struct. **245**, 183 (1991).
[7] R. L. Brinkley and R. B. Gupta, Ind. Eng. Chem. Res. **37**, 4823 (1998).
[8] F. P. S. C. Gil, R. Fausto, A. M. A. da Costa, and J. J. C. Teixeira-Dias, J. Chem. Soc., Faraday Trans. **90**, 689 (1994).
[9] F. P. S. C. Gil and J. C. Teixeira-Dias, J. Mol. Struct. **332**, 269 (1995).
[10] H. Yoshida, K. Takikawa, K. Ohno, and H. Matsuura, J. Mol. Struct. **299**, 141 (1993).
[11] X. H. Zhou, E. D. Huang, L. C. Zhong, S. Y. Liu, S. Z. Ma, H. W. Li, X. M. Yang, and W. R. Dong, J. Mol. Struct. **1294**, 136389 (2023).
[12] Y. Matsuda, N. Mikami, and A. Fujii, Phys. Chem. Chem. Phys. **11**, 1279 (2009).
[13] Y. J. Hu, J. W. Guan, and E. R. Bernstein, Mass Spectrom. Rev. **32**, 484 (2013).
[14] G. Li, Y. Y. Zhang, Q. M. Li, C. Wang, Y. Yu, B. B. Zhang, H. S. Hu, W. Q. Zhang, D. X. Dai, G. R. Wu, D. H. Zhang, J. Li, X. M. Yang, and L. Jiang, Nat. Commun. **11**, 5449 (2020).
[15] M. Miyazaki, A. Fujii, T. Ebata, and N. Mikami, Science **304**, 1134 (2004).
[16] H. L. Han, C. Camacho, H. A. Witek, and Y. P. Lee, J. Chem. Phys. **134**, 144309 (2011).
[17] H. B. Fu, Y. J. Hu, and E. R. Bernstein, J. Chem. Phys. **124**, 024302 (2006).
[18] Y. Matsuda, M. Mori, M. Hachiya, A. Fujii, and N. Mikami, Chem. Phys. Lett. **422**, 378 (2006).
[19] M. Katada, R. Shishido, and A. Fujii, Phys. Chem. Chem. Phys. **16**, 7595 (2014).
[20] Y. Matsuda, K. Hoki, S. Maeda, K. I. Hanaue, K. Ohta, K. Morokuma, N. Mikami, and A. Fujii, Phys. Chem. Chem. Phys. **14**, 712 (2012).
[21] J. W. Guan, Y. J. Hu, M. Xie, and E. R. Bernstein, Chem. Phys. **405**, 117 (2012).
[22] J. Y. Feng, Y. P. Lee, C. Y. Zhu, P. J. Hsu, J. L. Kuo, and T. Ebata, Phys. Chem. Chem. Phys. **22**, 21520 (2020).
[23] T. Lu, *Molclus Program, Version 1.9.9.4*. http://www.keinsci.com/research/molclus.html (accessed on May 7, 2022).
[24] S. Grimme, J. Antony, S. Ehrlich, and H. Krieg, J. Chem. Phys. **132**, 154104 (2010).
[25] M. Sierka, A. Hogekamp, and R. Ahlrichs, J. Chem. Phys. **118**, 9136 (2003).
[26] S. Grimme, S. Ehrlich, and L. Goerigk, J. Comput. Chem. **32**, 1456 (2011).
[27] M. J. Frisch, G. W. Trucks, H. B. Schlegel, G. E. Scuseria, M. A. Robb, J. R. Cheeseman, G. Scalmani, V. Barone, G. A. Petersson, H. Nakatsuji, X. Li, M. Caricato, A. V. Marenich, J. Bloino, B. G. Janesko, R. Gomperts, B. Mennucci, H. P. Hratchian, J. V. Ortiz, A. F. Izmaylov, J. L. Sonnenberg, D. Williams-Young, F. Ding, F. Lipparini, F. Egidi, J. Goings, B. Peng, A. Petrone, T. Henderson, D. Ranasinghe, V. G. Zakrzewski, J. Gao, N. Rega, G. Zheng, W. Liang, M. Hada, M. Ehara, K. Toyota, R. Fukuda, J. Hasegawa, M. Ishida, T. Nakajima, Y. Honda, O. Kitao, H. Nakai, T. Vreven, K. Throssell, J. A. Jr. Montgomery, J. E. Peralta, F. Ogliaro, M. J. Bearpark, J. J. Heyd, E. N. Brothers, K. N. Kudin, V. N. Staroverov, T. A. Keith, R. Kobayashi, J. Normand, K. Raghavachari, A. P. Rendell, J. C. Burant, S. S. Iyengar, J. Tomasi, M. Cossi, J. M. Millam, M. Klene, C. Adamo, R. Cammi, J. W. Ochterski, R. L. Martin, K. Morokuma, O. Farkas, J. B. Foresman and D. J. Fox, *Gaussian 16 Revision A. 03*, Wallingford: Gaussian Inc., (2016).
[28] F. Neese, WIREs Comput. Mol. Sci. **2**, 73 (2012).
[29] K. Kimura, S. Katsumata, Y. Achiba, T. Yamazaki, S. Iwata, *Handbook of HeI Photoelectron Spectra of Fundamental Organic Molecules: Ionization Energies, Ab Initio Assignments, and Valence Electronic Structure for 200 Molecules*, Tokyo: Japan Scientific Societies Press, 268 (1981).
[30] F. P. Lossing, J. Am. Chem. Soc. **99**, 7526 (1977).
[31] H. W. Biermann and T. H. Morton, J. Am. Chem. Soc. **105**, 5025 (1983).
[32] C. C. Van de Sande and F. W. McLafferty, J. Am. Chem. Soc. **97**, 4617 (1975).
[33] D. J. McAdoo, C. E. Hudson, V. M. S. Ramanujam, and M. George, Org. Mass Spectrom. **28**, 1210 (1993).

DOI: 10.1063/1674-0068/cjcp2403045